Nanopore-Based Assay for Detection of Methylation in Double-Strand DNA Fragments.

ARTICLE *in* ACS NANO · JANUARY 2015

Impact Factor: 12.88 · DOI: 10.1021/nn5045596 · Source: PubMed

10 AUTHORS, INCLUDING:

Jiwook Shim
University of Illinois, Urbana-Champaign
33 PUBLICATIONS **410** CITATIONS
SEE PROFILE

Younghoon Kim
University of Illinois, Urbana-Champaign
21 PUBLICATIONS **692** CITATIONS
SEE PROFILE

Ann M Nardulli
University of Illinois, Urbana-Champaign
70 PUBLICATIONS **2,680** CITATIONS
SEE PROFILE

Nanopore-Based Assay for Detection of Methylation in Double-Stranded DNA Fragments

Jiwook Shim,[†,‡] Younghoon Kim,[†] Gwendolyn I. Humphreys,[§] Ann M. Nardulli,[§] Farhad Kosari,[∥,⊥] George Vasmatzis,[∥,⊥] William R. Taylor,[∥,⊥] David A. Ahlquist,[∥,⊥] Sua Myong,[†] and Rashid Bashir*[,†,‡,⊥]

[†]Department of Bioengineering, [‡]Micro and Nanotechnology Laboratory, and [§]Department of Molecular and Integrative Physiology, University of Illinois at Urbana—Champaign Urbana, Illinois 61801, United States, [∥]Department of Molecular Medicine, Center for Individualized Medicine, Mayo Clinic, Rochester, Minnesota 55905, United States, and [⊥]Mayo—Illinois Alliance for Technology Based Healthcare

ABSTRACT DNA methylation is an epigenetic modification of DNA in which methyl groups are added at the 5-carbon position of cytosine. Aberrant DNA methylation, which has been associated with carcinogenesis, can be assessed in various biological fluids and potentially can be used as markers for detection of cancer. Analytically sensitive and specific assays for methylation targeting low-abundance and fragmented DNA are needed for optimal clinical diagnosis and prognosis. We present a nanopore-based direct methylation detection assay that circumvents bisulfite conversion and polymerase chain reaction amplification. Building on our prior work, we used methyl-binding proteins (MBPs), which selectively label the methylated DNA. The nanopore-based assay selectively detects methylated DNA/MBP complexes through a 19 nm nanopore with significantly deeper and prolonged nanopore ionic current blocking, while unmethylated DNA molecules were not detectable due to their smaller diameter. Discrimination of hypermethylated and unmethylated DNA on 90, 60, and 30 bp DNA fragments was demonstrated using sub-10 nm nanopores. Hypermethylated DNA fragments fully bound with MBPs are differentiated from unmethylated DNA at 2.1- to 6.5-fold current blockades and 4.5- to 23.3-fold transport durations. Furthermore, these nanopore assays can detect the *CpG* dyad in DNA fragments and could someday profile the position of methylated *CpG* sites on DNA fragments.

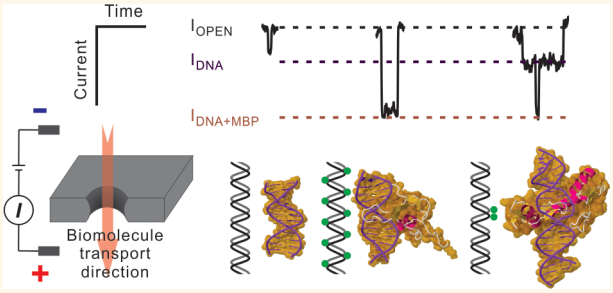

KEYWORDS: methylated DNA · methyl-binding protein · cancer detection · nanopore · single-molecule detection

Epigenetic alterations involving DNA methylation, which include addition and/or removal of a methyl group at the 5-position of cytosine, are early and frequently observed events in carcinogenesis.[1−3] Aberrant methylation occurs in the promoter sequences of various genes linked to many tumors.[4−6] Hypermethylation is reported to be associated with cancers of the prostate, colon, lung, liver, breast, head and neck and further correlated with metastatic potential in many other tumor types.[4,6−10] Also, high-throughput methylation analysis has uncovered aberrant DNA methylation in both premalignant and malignant neoplasia.[11−14] Hypomethylation is reported to be associated with cancers of the kidney, stomach, liver, colon, pancreas, uterus, cervix, and lung.[12,15−22] Thus, methylation analysis in DNA can play a critical role in the diagnosis of cancer, especially at an early, precancerous stage.

Previous studies have demonstrated the feasibility of detecting cancer by assessing methylation patterns from genomic extracts of body fluids such as plasma, serum, urine, and stool.[4,23−25] However, the level of methylated DNA in these fluids is extremely low,[26] and the size of the DNA fragments is quite small.[27] As a result, most conventional methylation assays require large sample volumes. In addition to the DNA fragmentation that occurs *in vivo*, bisulfite conversion can lead to further DNA degradation,[28,29] which additionally compromises the detection sensitivity of conventional methylation detection assays. Finally, most current assays employ polymerase chain reaction (PCR) amplification, which can introduce false-positive results.[4]

* Address correspondence to rbashir@illinois.edu.

Received for review August 14, 2014 and accepted January 8, 2015.

Published online January 08, 2015
10.1021/nn5045596

Thus, a simple, rapid, and reliable method to detect epigenetic modification of DNA, which uses small samples and eliminates bisulfite treatment and PCR amplification, has potential to revolutionize cancer diagnostics.

Here, we demonstrate a novel strategy to detect varying levels of methylation levels on double-stranded (ds) DNA using a solid-state nanopore-based sensor. The nanopore has been adapted to explore many biophysical questions through single-molecule investigation[8,30−38] and in applications toward next generation DNA sequencing.[39,40] A single-molecule detection technology using a nanopore sensor could be well-suited for gene-based methylation analysis,[33,41] and here we demonstrate the capacity of nanopore sensors to detect methylation in 30, 60, and 90 bp double-stranded oligos. This approach could be compatible with small amounts of genomic extracts and direct methylation detection without fluorescence labeling and bisulfite conversion. When integrated with sample preparation, the use of nanopore-based discrimination of various methylation patterns could provide a simple and affordable approach to early cancer detection.

RESULTS AND DISCUSSION

Discrimination of a Variety of Methylation Levels in DNA Fragments. Nanopore-based sensors can detect single molecules as they traverse through a nanopore and alter the background ionic current. Using the principle of electrical current spectroscopy to interrogate biomolecules at the single-molecule level, the sensors can discern subtle structural motifs through sensitive detection of electrical current signatures. The cross-sectional view of a solid-state nanopore is illustrated in Figure 1a. A focused electron beam is used to drill a nanopore within a thin dielectric membrane such as SiN, Al_2O_3, or HfO_2.[33,42,43] Two reservoir chambers clamp the nanopore membrane from both sides to create a giga-Ohm seal between the two chambers, making the nanopore the only single path of ionic current. The two reservoir chambers contain an electrolyte solution, and the charged single molecules are transported through the nanopore when a bias voltage is applied across the two chambers. Discrimination of the methylation state of 90 bp dsDNA oligos was first demonstrated at the single-molecule level using solid-state nanopores. Figure 1b,c shows representative single-molecule transport events. Two distinct nanopore current signatures were observed; the shallow events correspond to transport of naked DNA (left events in Figure 1b,c), and the deeper events correspond to the transport of bound protein (right events in Figure 1b,c). The target dsDNA utilized comprised unmethylated dsDNA (unMethDNA, Figure 1d), hypermethylated dsDNA (hyMethDNA) with 10 methylated *CpGs* uniformly distributed through the DNA

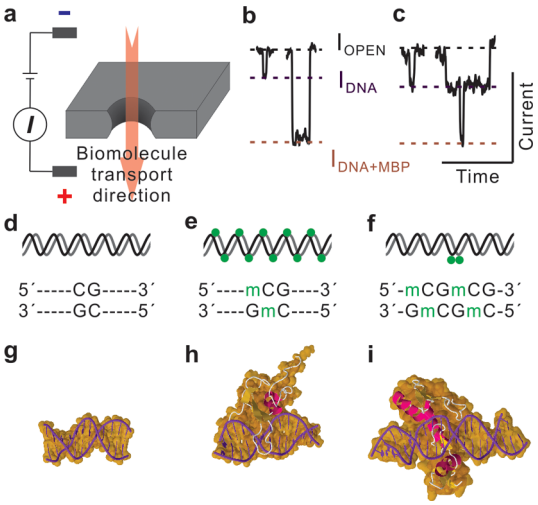

Figure 1. (a) Cross-sectional view of solid-state nanopore and biomolecule transport direction across the nanopore along the bias voltage. (b) Representative nanopore electrical current signatures of 90 bp unmethylated dsDNA (left) and hypermethylated dsDNA fully bound with methyl-*CpG*-binding protein (right). (c) Comparison of nanopore transport events between 90 bp unmethylated dsDNA (left) and locally methylated dsDNA bound with a single methyl-binding protein (right). Schematics of 90 bp dsDNA fragments showing (d) unmethylation, (e) hypermethylation, and (f) local methylation. Crystal structures of (g) bare B-form dsDNA (PDB ID: 1BNA), (h) methyl-*CpG*-Binding domain protein bound to a symmetric *CpG* dinucleotide on dsDNA (PDB ID: 1IG4), and (i) Kaiso zinc finger protein bound to two symmetric adjacent *CpGs* on dsDNA (PDB ID: 4F6N).

sequence (Figure 1e), or locally methylated dsDNA (loMethDNA) with two repetitive methylated *CpGs* at the center of the sequence (Figure 1f). The DNA sequence of the unMethDNA was identical to that of the hyMethDNA and loMethDNA sequences but contained no methylated sites. Each of the DNA sequences used in this report is shown in Supporting Information Table S1. Methylation sites in DNA fragments were labeled with methyl-binding proteins (MBPs). Two types of MBPs were used for labeling: MBD1x and KZF. Electrophoretic mobility shift assays for methylated DNA and MBP interactions are shown in Supporting Information Figure S1. These MBPs recognize and bind specifically to methylated *CpGs*; MBD1x is the key methyl-*CpG*-binding domain of methyl-*CpG*-binding domain protein (MBD),[44] and KZF is the key methylation binding domain of Kaiso zinc finger (KZF) protein.[45] Kaiso is a Cys2−His2 zinc finger protein that binds to methylated CpG and a sequence-specific DNA target. The sequence of KZF contains all three fingers (*aa472−573*).[45] The sequence excludes the extra C-terminal domain to prevent nonspecific binding on DNA because some C2H2 KZF utilizes extra domains for nonspecific binding on DNA.[46] In a similar fashion, Kaiso contains an arginine/lysine-rich region on its C-terminal end, which forms structured loops upon DNA binding that stabilize the contact but also increase nonspecific target binding. The small dimensions of

these MBPs contribute to making nanopore-based detection feasible for naked DNA. MBD1x spans 5−6 bps on DNA upon binding and has a molecular weight of 16.3 kDa,[44] and KZF wraps around 5−6 bps of DNA and has a molecular weight of 13.02 kDa.[45] The crystal structure of typical B-form DNA[47] is shown in Figure 1g, and the two MBPs on methylated DNA are shown in Figure 1h for MBD1x[48] and Figure 1i for KZF.[45] The MBPs were incubated with methylated DNA at room temperature for 15 min to form the methylated DNA/MBP complex prior to the nanopore-based methylation assay. The passage of the MBP-bound methylated DNA through the nanopore resulted in a significantly different current signature compared to the passage of naked DNA. Because the pore current blockade depends on the cross-sectional diameter of the translocating molecule, a deeper current blockade should be observed when the protein-bound DNA traverses the nanopore (shown in Figure 1b,c). Nanopore-based single-molecule detection through sub-10 nm nanopores identified different methylation profiles (shown in Figure 1d−f for unmethylated, hypermethylated, and locally methylated, respectively) on the dsDNA fragment with significantly different electrical current signatures. The hyMethDNA/MBD1x complex could be distinguished from unMethDNA by the prolonged translocation time (Δt) and increased current blocking (Figure 1b). The loMethDNA/KZF complex transport also produced prolonged Δt and stepwise current blocking (Figure 1c). The extended transport duration of the DNA/complexes was attributed to the net positive charge of MBD1x and KZF in the pH 7.6 nanopore assay buffer solution, which helped to reduce the velocity of complex transport through the negatively charged SiN nanopore.

This methylated DNA detection method does not require bisulfite conversion and PCR amplification as is required for conventional methylation detection[29] or fluorescent tags that are required for optical analysis.[49] Rather, this nanopore-based detection method relies on direct, single-molecule electrical detection. Consequently, nanopore-based methylated DNA detection could be significantly useful in rapid screening for epigenetic biomarkers.

Selective Detection of Hypermethylation. A nanopore relatively larger than the dimension of a methylated DNA fragment fully bound with MBD1x was utilized for the selective detection of hyMethDNA/MBD1x. The transmission electron microscopy (TEM) image of a 19 nm nanopore fabricated in a 10 nm thick SiN membrane (Norcada, Alberta, Canada) is shown in Figure 2a. A 10 nM concentration of 90 bp unMethDNA was introduced in the nanopore for investigation of single-molecule translocation through a 19 nm nanopore. In this large nanopore, the ionic signature of DNA-only transport was not observed, unlike typical dsDNA transport through a smaller diameter nanopore, as

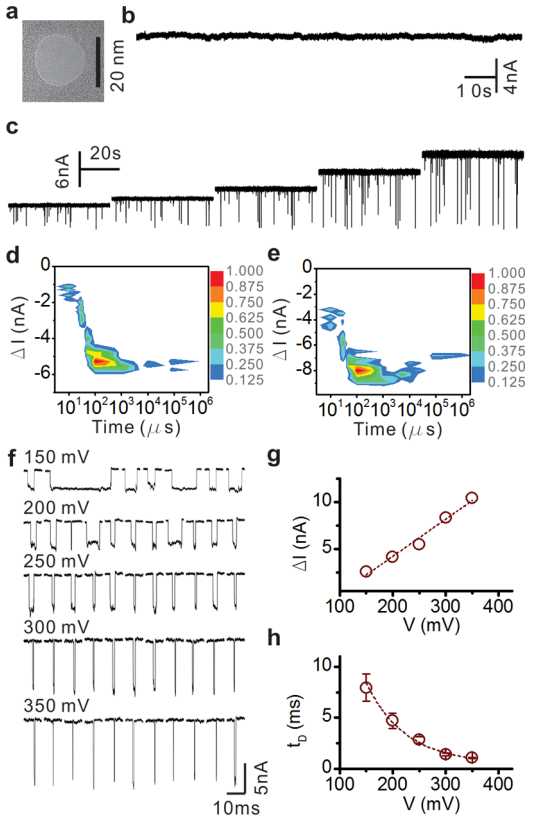

Figure 2. (a) TEM image of a 19 nm nanopore. (b) Nanopore current trace of 90 bp unMethDNA transports at 200 mV driving force. No noticeable events are observed. (c) Nanopore current traces show transports of 90 bp hyMethDNA/MBD1x complexes. Data traces from left to right are recorded in a range of 150 and 350 mV with increments of 50 mV. Contour plots show transports of hyMethDNA/MBD1x at (d) 250 mV and (e) 300 mV. (f) Representative single-molecule transport events of hyMethDNA/MBD1x complex at various voltages. The number of events used for the analysis is 235 at 150 mV, 252 at 200 mV, 255 at 250 mV, 326 at 300 mV, and 341 at 350 mV. (g) Current blockade of complex transports. Each value is obtained by fitting the Gaussian function to a current blocking histogram. The obtained values of current blockades are 2.43 ± 0.05, 3.55 ± 0.06, 5.2 ± 0.04, 7.69 ± 0.08, and 9.51 ± 0.07 nA from 150 to 350 mV. The trend line in short dashes is obtained by fitting first-order polynomial values, indicating an increase of current blocking at higher bias voltages. (h) Transport duration of the complex. Each value is obtained by fitting the exponential decay to a transport time histogram. The obtained values of transport duration are 7.96, 4.72, 2.83, 1.43, and 1.06 ms from 150 to 350 mV, and the values are fitted well with exponential decay function as shown in the short dashed trend line, indicating voltage dependency of transport duration.

shown in Supporting Information Figure S2. The nanopore ionic current signature of unnoticeable unMethDNA transports recorded at 200 mV is shown in Figure 2b. In contrast, a series of significant nanopore current blockades are observed after adding a mixture containing 100 pM of hyMethDNA/MBD1x complex and 10 nM unMethDNA to the nanopore. The selective detection of hyMethDNA/MBD1x complex over unMethDNA through a 19 nm nanopore can be explained by rapid translocation velocity and a largely unoccupied nanopore

with unMethDNA. Smeets *et al*. demonstrated translocation of 5k and 48.5k dsDNAs through a 24.2 nm nanopore, and the translocation velocity of those molecules was obtained at 0.173 and 0.039 μs/bp, respectively.[50] The calculated translocation duration of 90 bp according to the velocity from these previous studies is ~9.54 μs/molecule, which is undetectable from our recording sampling rate at 10 μs (see Materials and Methods). Also, the current blockade of dsDNA of 2.2 nm diameter in a 19 nm nanopore is calculated to only be 1.2%, using the equation $\Delta I = (a/d)^2$, where a and d are diameters of the molecule and the nanopore, respectively. With ~20 nA open pore current with ~500 pA peak-to-peak baseline noise (Supporting Information Figure S3), the calculated current blockade of dsDNA at ~240 pA is clearly undetectable. Meanwhile, the relatively larger diameter of the hyMethDNA/MBD1x complexes induces significant current blockade with larger blocked current during a prolonged translocation. Similar findings were reported with a RecA protein-coated dsDNA filament *versus* dsDNA alone.[50] Due to an undetectable quick and shallow nanopore ionic current blockade of unMethDNA, the nanopore exclusively detected hyMethDNA bound to MBD1x in the mixture with unmethylated DNA. Also, our previous study proved that unbound MBD1x is positively charged at pH 7.6 of nanopore buffer solution, thus transport of unbound MBD1x is not observed at positive driving voltage across the nanopore.[33] Consequently, a 19 nm nanopore can selectively detect translocation of the complexes and can screen the presence of methylated DNA in mixed sample solution. Representative long-term recordings of current blockades induced by transport of hyMethDNA/MBD1x complexes from 150 to 350 mV are shown in Figure 2c from left to right. Contour plots of complex transport events at 250 and 300 mV are shown in Figure 2d,e, respectively. The wide spread of the current blockade in contour plots may be explained by unsuccessful DNA threading attempt,[51] and by differing levels of methylation in single dsDNA molecules, as shown in a gel shift assay (Supporting Information Figure S1 and previous study[33]). However, the majority of current blockades fall into one group, indicating that most events involve complex transport and most complexes contain a fairly equal number of MBD1x. The representative transport events of single-molecule hyMethDNA/MBD1x are shown in Figure 2f. The analyses of hyMethDNA/MBD1x complex transport through a 19 nm nanopore are presented in Figure 2g,h for transport current blockade and transport duration. Values of current blockades were obtained by fitting the histogram of all blocked currents induced at each applied voltage to a Gaussian function, and the values of translocation duration were obtained by fitting the histogram of all blocked currents' duration to an exponential decay function. The short dashed trend line of current blockade values is fitted with a first-order polynomial function, indicating that conductance blockades increase at higher applied voltages. The short dashed trend line of transport duration values is fitted with an exponential decay function, indicating that the transport velocity is voltage-dependent. In summary, hypermethylated 90 bp DNA was specifically labeled with MBD1x, and the presence of hyMethDNA in a mixture with unMethDNA was selectively detected at the single-molecule level using a 19 nm diameter solid-state nanopore. This method could find initial applications in screening for the presence of hypermethylated DNA in a mixture.

Differentiation of Hypermethylation from Unmethylated DNA. The methylation patterns of human genomic DNA has recently been detected by collecting DNA on MBD chromatography columns after digesting methylated DNA into fragments with the restriction enzyme MseI.[52] Herein, we further demonstrate the detection of hypermethylation using 30, 60, and 90 bp dsDNA. The hyMethDNA fragments contained 10% methylated *CpG*s uniformly distributed along the entire sequence, while unMethDNA fragments possessed no methylation. Nanopores with diameters ranging from 7.1 to 9.5 nm are utilized to detect methylated dsDNA. We demonstrated the discrimination of hypermethylated and nonmethylated DNA fragments. First, 90 bp dsDNA fragments in a mixture (100 pM for both hyMethDNA and unMethDNA) were analyzed through a 7.7 nm diameter nanopore. The nanopore ionic current in Figure 3a shows mixed transport events of 90 bp hyMethDNA (fully bound with MBD1x) and unMethDNA recorded at 300 mV. The nanopore with diameter comparable with the dimension of hyMethDNA/MBD1x complex clearly detected transport events of the unMethDNA and hyMethDNA/MBD1x. The cross-sectional diameter of hyMethDNA/MBD1x was ~5 nm when a single protein bound to DNA and ~7.6 nm with multiple bound proteins, as also shown in a previous study.[33] The scatter plot of all mixed single-molecule transport events is shown in Figure 3b and presents prolonged-deeper current blockade of hyMethDNA/MBD1x transports (Figure 3c) along with fast-shallow current blockage from transport of unMethDNA (Figure 3d). A contour plot of Figure 3b is provided to show two major distinct event populations for naked DNA and the DNA complex transports (Supporting Information Figure S4). In comparison with the scatter plots of mixed events through the 19 nm nanopore shown in Figure 2d,e, unMethDNA and hyMethDNA/MBD1x are clearly discriminated using the 7.7 nm nanopore: the shallow current blocking events from unMethDNA and deep current blocking events from hyMethDNA/MBD1x. To confirm that the fast-shallow events in the mixture are the single-molecule transport of unMethDNA, a separate

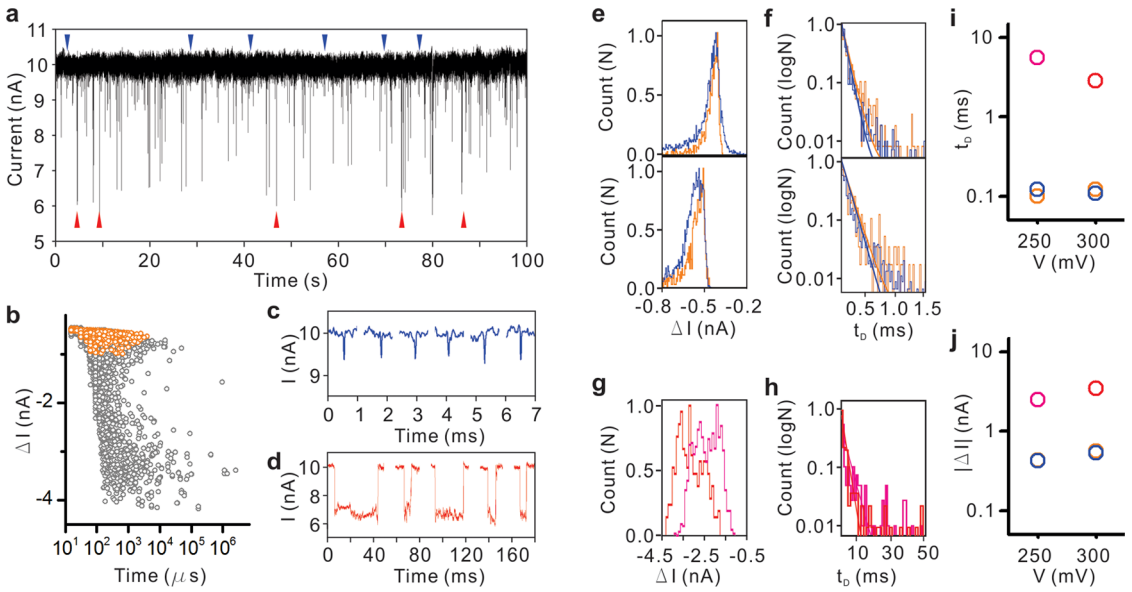

Figure 3. (a) Nanopore current trace shows mixture transports of 90 bp long unMethDNA and hyMethDNA/MBD1x complex, recorded at 300 mV in 1 M KCl containing 10 mM Tris and 1 mM ethylenediaminetetraacetic acid at pH 7.6. (b) Scatter plot in gray color shows mixture events of 90 bp long unMethDNA and hyMethDNA/MBD1x complex and in orange color shows 90 bp long unMethDNA-only events obtained from separate experiment. Separate unMethDNA-only events match well with fast-shallow current blocking events found in the mixture, indicating that the fast-shallow events of the mixture represent transport of 90 bp unMethDNA. (c) Representative sample transports of unMethDNA marked with inverted blue triangles in (a). (d) Representative sample transport events of hyMethDNA/MBD1x complex marked with red triangles in (a). (e) Current blocking histograms of unMethDNA transports recorded at 250 mV (top) and 300 mV (bottom). (f) Transport duration histograms recorded at 250 mV (top) and at 300 mV (bottom). Events obtained from the mixture are in blue, and separate unMethDNA-only are in orange for both (e) and (f). (g) Current blocking histogram of hyMethDNA/MBD1x complex transports. (h) Transport duration histogram of hyMethDNA/MBD1x complex transports. The histograms are built with prolonged-deep current blocking events in mixture transports, as shown in (d), recorded at 250 mV (pink) and at 300 mV (red) for (g) and (h). (i) Transport duration values of unMethDNA and hyMethDNA/MBD1x complexes. Each point is obtained by fitting the transport duration histogram to an exponential decay. Transport durations of unmethylated dsDNA are in a range between 100 and 125 μs, while complex transports are in a prolonged duration of 5.59 and 2.86 ms at 250 and 300 mV. (j) Current blockade values obtained by fitting the Gaussian function to the current blockings. Current blockade of unMethDNA transports are ∼0.45 nA at 250 mV and ∼0.56 nA at 300 mV, while hyMethDNA/MBD1x complexes block current of ∼2.5 nA at 250 mV and ∼3.5 nA at 300 mV. The number of events used for these analyses was 2135 for the mixture and 841 for separate unMethDNA at 250 mV and 1860 for the mixture and 613 for unMethDNA at 300 mV.

investigation of unMethDNA single-molecule transport through the same nanopore was performed and a scatter plot of pure unMethDNA transport events is superimposed on the scatter plot of mixed events. The analysis of separate unMethDNA transport and fast-shallow events in mixed molecule transport showed good agreement in current blockades and transport durations. Histograms of transport durations and current blockades were obtained from mixtures and separate unMethDNA current traces recorded at 250 and 300 mV, as shown in Figure 3e,f. The values of transport duration of unmethylated DNA were obtained by fitting the transport duration histogram to an exponential function. Both transport durations of unMethDNA and fast-shallow events in mixed solution ranged between 100 and 125 μs at 250 and 300 mV. Current blockades were obtained by fitting the current blocking of events to a Gaussian function. Single-molecule transport of unMethDNA blocked a current of 0.433 nA at 250 mV and 0.561 nA at 300 mV, and fast-shallow events blocked a current of 0.429 nA at 250 mV and 0.537 nA at 300 mV. Consequently, the fast-shallow events in mixed solution represent single-molecule transport of unMethDNA through the nanopore rather than collisions of the complex at the entrance of the solid-state nanopore. Representative nanopore electrical signatures of single-molecule unMethDNA transport and single-molecule hyMethDNA/MBD1x complex transport in mixed events are shown in Figure 3c,d. The analysis of hyMethDNA/MBD1x single-molecule transport events showed ∼2.5 and ∼3.5 nA current blocking, obtained by fitting the histogram in Figure 3g to a Gaussian function. The analysis also showed 5.59 and 2.86 ms transport duration at 250 and 300 mV, obtained by fitting the histogram in Figure 3h to an exponential decay function. The comparison between hyMethDNA/MBD1X and unMethDNA is shown in Figure 3i for transport times and Figure 3j for current blockades. A hypermethylated DNA bound with MBD1x is clearly distinguishable from the signatures of the unMethDNA events.

Various length DNA fragments were also used to discriminate 10 pM of hyMethDNA fully bound with MBD1x in 1 nM of unMethDNA through nanopore ionic signatures of current blockage and duration.

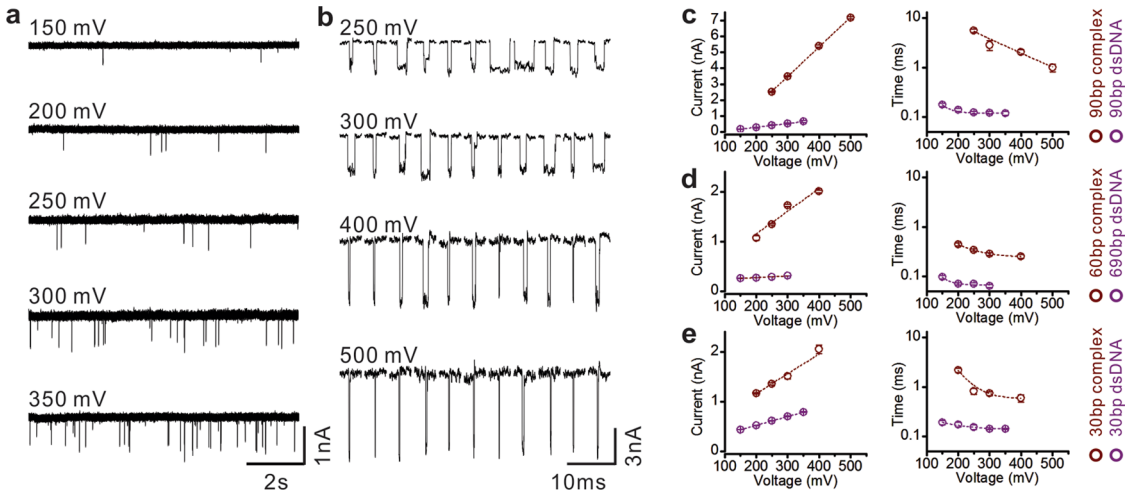

Figure 4. (a) Representative nanopore ionic current traces of unMethDNA (concentration at 1 nM) transports. (b) Representative sample single-molecule transport events from raw traces of hyMethDNA/MBD1x complex (concentration at 10pM) transports. (c) 90 bp long hyMethDNA/MBD1x complex and unMethDNA transports (unMethDNA events, *n* = 1225 at 150 mV, 1866 at 200 mV, 1136 at 250 mV, 741 at 300 mV, and 436 at 350 mV; hyMethDNA/MBD1x events, *n* = 963 at 250 mV, 943 at 300 mV, 605 at 400 mV, and 848 at 500 mV). (d) 60 bp long hyMethDNA/MBD1x complex and unMethDNA (unMethDNA events, *n* = 2135 at 150 mV, 1613 at 200 mV, 1088 at 250 mV, and 787 at 300 mV; hyMethDNA/MBD1x events, *n* = 336 at 200 mV, 503 at 250 mV, 549 at 300 mV, and 505 at 400 mV). (e) 30 bp long hyMethDNA/MBD1x complex and unMethDNA (unMethDNA events, *n* = 1167 at 150 mV, 578 at 200 mV, 788 at 250 mV, 681 at 300 mV, and 781 at 350 mV; hyMethDNA/MBD1x events, *n* = 160 at 200 mV, 132 at 250 mV, 198 at 300 mV, and 126 at 400 mV). HyMethDNA/MBD1x complex transports are in brown, and unMethDNA transports are in purple. The values of the current blockade are shown in the left panel, and the values of transport duration are shown in the right panel for (c–e). The short dashed trend lines for current blockade are obtained by fitting the first-order polynomial, indicating an increased current blockade at higher driving force. The short dashed trend lines for transport duration are obtained by fitting to the exponential decay, indicating voltage-dependent translocation velocity.

TABLE 1. Comparison of Experimental Results of unMethDNA and hyMethDNA/MBD1x at Various Lengths[a]

DNA length	no. of mCpG	nanopore diameter (nm)	DNA current blockage (nA)	complex current blockage (nA)	complex/ DNA	DNA transport duration (ms)	complex transport duration (ms)	complex/ DNA
90 bp	10	7.70	0.54	3.50	6.52	0.12	2.86	23.33
60 bp	6	9.50	0.31	1.73	5.54	0.06	0.29	4.45
30 bp	3	7.10	0.71	1.51	2.14	0.14	0.74	5.14

[a] Values are extracted from transport events recorded at 300 mV.

Representative current traces of unMethDNA and sample events of hyMethDNA/MBD1x are shown in Figure 4a,b. Analyses of single-molecule transport of unMethDNA and hyMethDNA/MBD1x are compared in Figure 4c–e for 90, 60, and 30 bp DNA fragments. In each panel, the left graph shows the current blockade difference and the right graph shows the transport duration difference between unMethDNA (in purple) and hyMethDNA/MBD1x complex (in brown). The trend line of current blockades is fitted by a first-order polynomial function, and the trend line of transport times is fitted with an exponential decay function. These trends are shown as short dashed lines in Figure 4c–e and are consistent with previous findings where conductance blockades of DNA translocation increase in depth at increased applied voltages[33,53] and reduce in duration in a voltage-dependent manner as applied voltage increases.[51] Specifically at 300 mV, 90 bp hyMethDNA/MBD1x was discriminated from 90 bp unMethDNA by a 6.5-fold difference in current blocking and a 23-fold difference in transport duration; 60 bp hyMethDNA/MBD1x demonstrated 5.5-fold current blocking and 4.5-fold transport duration over 60 bp unMethDNA, and 30 bp hyMethDNA/MBD1x demonstrated 2.1-fold current blocking and 5.1-fold transport duration as compared to 30 bp unMethDNA. The comparison of single-molecule transport events between complex and unMethDNA recorded at 300 mV is shown in Table 1. Interestingly, the 90 bp hyMethDNA with 10 MBD1x shows significantly prolonged transport times compared to 30 bp hyMethDNA with 3 MBD1x through nanopores of similar diameters (see Table1). Interaction between MBD1x (on the DNA) and the surface of a nanopore with the opposite charge was reported to slow the translocation of hyMethDNA/MBD1x complexes through a nanopore.[33] Consequently, more MBD1x-associated DNA has longer transport time. To confirm this interaction, single-molecule transport events of 90 bp hyMethDNA fully bound with MBD1x through 19 and 7.7 nm

nanopores are also compared (Supporting Information Figure S5). Transport durations of hyMethDNA/MBD1x through 7.7 nm are 5.59 and 2.86 ms and through the 19 nm pore are 2.83 and 1.43 ms at 250 and 300 mV, respectively. Stronger interactions between the protein and the surface of the narrow nanopore (7.7 nm) slow the translocation durations of complexes by 2-fold compared to the larger nanopore (19 nm) at 250 and 300 mV.

Detection of a *CpG* Dyad in Short dsDNA. The patterns of DNA epigenetic alterations in cancer vary from the individual *CpG* dyad at the local level to methylations in 1 million base pairs, or DNA demethylation during carcinogenesis which results in loss of methylation on both strands *via* possible intermediates of hemi-methylated dyads.[54] Although reduced methylation in DNA (hypomethylation) compared to a normal level is another major epigenetic modification in cancer cells, diagnosis of DNA hypomethylation using conventional techniques such as methylation-specific PCR is technically limited and challenging.[55] Herein, a nanopore-based methylation assay demonstrates detection of reduced methylation at the local level single *CpG* dyad in the DNA fragment. We utilize KZF to detect local methylation in DNA fragments with its relevance to cancer and high binding affinity to methylated *CpG*s. KZF demonstrates high binding affinity of K_d = 210 ± 50 pM, forming 1:1 complexes with single consecutive methylated *CpG*s,[45] and is reported to bind and silence aberrantly methylated DNA repair genes and tumor suppression in cancer cells.[56] We chose two repetitive methylated *CpG*s to mimic the methylation pattern of hypomethylation occurring in normally methylated *CpG* islands in somatic tissues.[57] The target 90 bp loMethDNA fragments have 30 potential *CpG* methylation sites, but only two repetitive *CpG* sites at the center are methylated. The target fragments are also designed to have repeated sequences to mimic the hypomethylation occurring in repeated sequences of genomic DNA.[54] The crystal structure of engineered KZF bound on DNA methylated sites is shown Figure 5a (side view) and Figure 5b (top-down view).[45] This loMethDNA bound with KZF is discriminated from unMethDNA with different nanopore ionic current events. We utilized a nanopore for which the diameter tightly fits with the width of loMethDNA/KZF complex. The width of the complex is 4.9 nm, and the diameter of the nanopore used was 5.5 nm, as shown in Figure 5b,c. The nanopore current trace of loMethDNA/KZF at 10 pM mixed unMethDNA at 1 nM and is shown in Figure 5d, showing significantly distinct current blockades. A representative nanopore electrical signature of single-molecule unMethDNA transport and an all-point histogram of transport events are shown in Figure 5e, and current events of loMethDNA/KZF transport are shown in Figure 5f, with the all-point histogram in the right

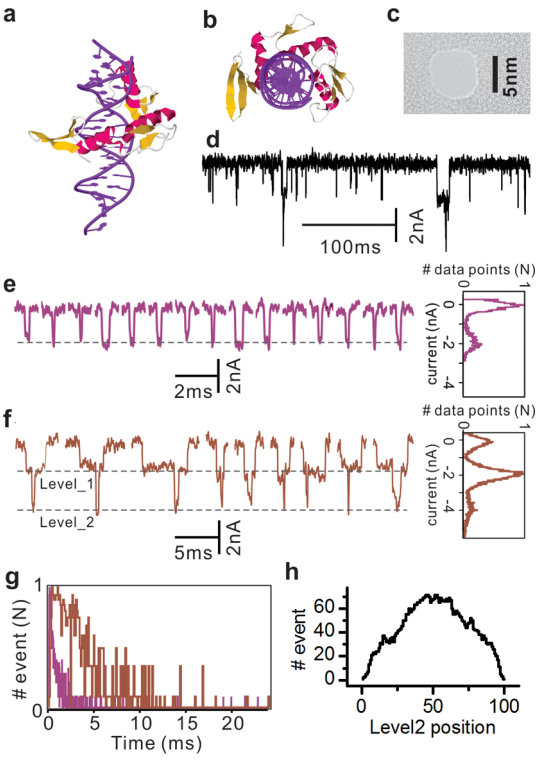

Figure 5. (a) Side view of crystal structure that describes loMethDNA bound with a single KZF (PDB ID: 4F6N). (b) Top-down view of loMethDNA/KZF complex. Dimension of the complex is measured at 4.9 nm from end to end of KZF bound on loMethDNA. (c) TEM image of a 5.5 nm diameter nanopore. (d) Nanopore ionic current trace of mixture transports between 1 nM of 90 bp long unMethDNA and 10 pM of 90 bp long loMethDNA/KZF complex. (e) Representative sample single-molecule transports of unMethDNA and all-point histogram (right, *n* = 50), demonstrating open pore current and current blockade of unMethDNA transports. (f) Representative transport events of loMethDNA/KZF complex and all-point histogram (right, *n* = 20). Current blockades in two obvious levels are observed; shallow blockade is attributed to the dsDNA region and the deeper blockade to the protein−DNA region in complex. (g) Transport duration histograms of unMethDNA (in purple) and loMethDNA/KZF complex (in brown). (h) Deeper current blockade position profile of complex transport events. The number of events used for this analysis was 7497 for unMethDNA and 379 for loMethDNA/KZF complexes.

panel. Current blockade histograms with all events are presented in Supporting Information (Figure S7). Current blockade of the loMethDNA/KZF complex showed two distinct levels; the shallow current blockade of ~2 nA is attributed to transport of the DNA-only region of the complex, and the deeper blockage of ~4 nA is attributed to the region of DNA bound with KZF in complex. The peak of the shallow current blockade in the all-point histogram in Figure 5f is well matched with the peak current blockade of unMethDNA transport in Figure 5e. Hence, the shallow blocking in loMethDNA/KZF can be attributed to the translocation of a protein-free DNA region in the complex through the nanopore. Our nanopore-based methylation assay discriminates loMethDNA bound with KZF at 2-fold current blockade and 5-fold

transport duration from unMethDNA. Current blockade of unMethDNA was obtained at 1.87 ± 0.02 nA, and loMethDNA/KZF was at 3.77 ± 0.03 nA. The histograms of transport duration of both unMethDNA and loMethDNA-MBD1x are shown in Figure 5g, and the fitted values of transport times from an exponential decay function are obtained at 0.19 ± 0.006 and 3.98 ± 0.32 ms, respectively. In addition, Figure 5f shows a stepwise current blockade with two current blocking levels. Level_2 current blockade was clearly distinguished from level_1, and solely obtained level_2 duration was at 0.33 ± 0.014 ms (Supporting Information Figure S8). The occurrence of level_2 current blockade was mainly observed at the center of the whole complex transport, as shown in Figure 5h. The *x*-axis represents the length of entire complex transport, normalized and recalculated as 100%. The peak occurrence of deeper current blockade was obtained by fitting a Gaussian function to the occurrence histogram, and the fitting value was 52.1%, indicating that a deeper current blockade mainly occurs at the middle of the entire complex translocation. These results provide very preliminary evidence that the position of methylated *CpG*s in loMethDNA could be profiled some day by analyzing the location of level_2 current blocking from the entire stepwise DNA complex translocation.

In summary, we utilized KZF to detect loMethDNA and to roughly determine the methylation location where the nanopore electrical current signature of loMethDNA/MBP demonstrated stepwise deeper current blocking, as shown in Figure 5f. This was significantly different from the prolonged single level deeper current blocking of hyMethDNA/MBP in Figure 2f and Figure 3c. Interestingly, KZF also has high binding affinity for symmetric single methylated *CpG* dinucleotides and hemimethylation of two adjacent *CpG*s in dsDNA with slightly reduced binding affinity.[45] With the versatile binding affinity of KZF to various methylation patterns, various patterns can be screened using our nanopore-based methylation assay.

CONCLUSION

We present a direct electrical analysis technique to detect various methylation levels on DNA fragments at the single-molecule level using solid-state nanopores. Hypermethylated DNA, a molecular-level epigenetic biomarker for cancer, can be selectively labeled using MBD1x as a methylation-specific label and can be detected without the need for any further processes, such as bisulfite conversion, tagging with fluorescent agent, or sequencing. The large nanopore successfully exhibited exclusive detection of methylated DNA bound to MBD1x in a mixture with unmethylated DNA. This method could find an initial application for screening the presence of hypermethylated DNA. Differentiation between hypermethylated and unmethylated dsDNA oligos was demonstrated using sub-10 nm nanopores, thus nanopore-based methylation assays also have the potential to identify abnormally methylated DNA in clinical tests aimed at diagnosis of diseases such as cancer. Hypomethylation in locally methylated *CpG* dyads is another epigenetic biomarker for cancer, and the methylated *CpG* dyads were labeled with KZF and discriminated from unmethylated DNA—hypomethylated DNA in this case. Furthermore, we could coarsely profile the methylation position in DNA. However, a nanopore-based methylation assay should improve the efficiency for low sample volume obtained from body fluids. Our next steps include integrating a nanopore-based assay in a microfluidic system to collect genomic DNA samples adjacent to the nanopore and detect methylation *in situ*. Bodily fluids, such as stool or blood, represent rich sources of genomic DNA that can be obtained non-invasively. DNA sequences can be hybrid-captured from such samples and concentrated near a nanopore integrated with a microfluidic system. Wanunu *et al.* showed successful nanopore detection of 1000 events in 15 min with a sample amount of 1 000 000 molecules/10 μL.[58] The relative percentage of aberrantly methylated DNA in stool samples from patients with colorectal cancer averages about 5% but can be much lower in some instances.[59] Using the approaches presented in this paper, the nanopore-based methylation detection method should be feasible for developing a new methylation assay from small volume samples. The next generation of methylation assay using an integrated nanopore in a microfluidic device could herald a revolution in rapid, accurate, and amplification-free methylation detection.

MATERIALS AND METHODS

Solid-State Nanopore, Chemicals, and Materials. The free-standing low-stress SiN membranes with 10 nm thickness and 50 × 50 μm^2 area, supported on a silicon substrate, were purchased from Norcada (Alberta, Canada). Single nanopores with various diameters were drilled with condensed electron beam using a JEOL 2010F field emission transmission electron microscope. All custom DNA fragments including methylation patterns for nanopore experiments were synthesized and purchased from Integrated DNA Technologies (Coralville, IA). The nanopore measurements were performed in 1 M KCl at pH 7.6 containing 10 mM Tris and 1 mM ethylenediaminetetraacetic acid (EDTA) for hypermethylated DNA fragments bound with MBD1x and in 0.2 M NaCl at pH 7.6 containing 10 mM Tris and 1 mM EDTA for locally methylated DNA fragments bound with KZF. The methylated DNA/MBP complexes were prepared and incubated for 15 min at room temperature (25 ± 2 °C) immediately before the nanopore experiment. Hypermethylated DNA was mixed with MBD1x in 80 mM KCl at pH 7.6 containing 10 mM Tris, 1 mM EDTA, and 0.4 mM DTT. The high ratio of MBD1x to methylated DNA was used to fully bind MBD1x to methylated DNA: ratio of 6:1 for 30 bp, 12:1 for 60 bp, and 20:1 for 90 bp methylated DNA.

Locally methylated DNA and KZF were mixed in equal ratio in 200 mM NaCl at pH 7.6 containing 10 mM Tris, 1 mM ZnCl, and 1 mM TCEP.

Nanopore Electrical Measurements. Nanopore chips were piranha-cleaned (two-thirds of 95% H_2SO_4 and one-third of 30% H_2O_2) for 10 min and thoroughly rinsed five times with large amount of deionized H_2O, and then the nanopore chip was clamped and sealed between two custom acrylic chambers to form the nanopore, the only electrical path of ions between the two reservoirs. Ag/AgCl electrodes were immersed in reservoirs for ionic current recordings. Axopatch 200B was used for applying potentials and measuring currents, and data were recorded using a Digidata 1440A data acquisition system. Nanopore current traces were recorded using a 10 kHz built-in low-pass Bessel filter and 10 μs sampling rates. Instrumental control and data analysis were performed using Clampex 10.2 and Clampfit 10.2. All data points of current blockage were obtained using Gaussian fit, and transport duration was determined using an exponential decay function in Clampfit 10.2 software. Also, all error bars were given with standard error obtained during the fitting. All nanopore experiments were performed in a dark double Faraday cage on an antivibration table at room temperature (25 $\pm$ 2 °C).

MBD1x Protein Purification. MBD1x purification was introduced in a previous report.[33]

Plasmid Construction. The Kaizo zinc finger DNA sequence was codon-optimized, PCR-amplified, and cloned into pUC19 (Fisher). The pUC19 plasmid was digested with Xma1 and subcloned into pQE80L (Quiagen) expression vector that was modified to contain mCherry and a thrombin cleavage site[60] and digested with *Xma*I (New England Biolabs) and calf intestinal alkaline phosphatase (New England Biolabs). The expression vector was transformed into DH5-alpha *Escherichia coli*, and positive colonies were checked by sequencing performed at the UIUC core sequencing facility.

KZF Protein Expression. The pQE80L expression vector containing mCherry−KZF was transformed into *E. coli* BL21(DE3)pLysS. An overnight culture of a single colony was grown in Luria-Bertani medium with ampicillin (100 μg/L). The culture was expanded into 1 L of Luria-Bertani broth with ampicillin, and at OD_{600} of 0.3, isopropyl-D-thiogalactopyranoside (1.0 mM) was added to the culture. Cell pellets were harvested by centrifugation at 6000*g* for 15 min at 4 °C and snap frozen.

KZF Protein Purification. Lysis buffer (20 mM Tris at pH 7.9, 0.1 mM $ZnCl_2$, 8 M urea, 10% v/v glycerol, 500 mM NaCl, 10 mM imidazole) was added to the cell pellet and incubated with lysozyme (1 mg/mL) at 4 °C for 1 h. The lysate was sonicated and then centrifuged at 10 000*g* at 4 °C for 1 h. The bacterial supernatant was added to a column packed with Ni-NTA resin for 1 h at 4 °C. The column was extensively washed with wash buffer (20 mM Tris at pH 7.9, 0.1 mM $ZnCl_2$, 10% v/v glycerol, 500 mM NaCl, 20 mM imidazole), and mCherry was cleaved by incubation with biotinlyated thrombin overnight at 4 °C. Excess biotinylated thrombin was removed by streptavidin-coated beads and centrifugation. Protein was diluted in TDZ buffer (20 mM Tris at pH 7.9, 0.1 mM $ZnCl_2$, 20% v/v glycerol) and injected into heparin column in an AKTA FPLC (GE HealthCare). The column was washed with 5−10 volumes of TDZ buffer with 200 mM NaCl, and the protein was eluted with TDZ buffer with q1 M NaCl; 70% glycerol was added, and the purified KZF protein was stored at −20 °C.

Conflict of Interest: The authors declare no competing financial interest.

Acknowledgment. The authors would like to acknowledge funding support from National Institutes of Health (R21 CA155863 to R.B. and NIDDK R01 053884 to A.N.). The authors would also like to acknowledge financial support from the Mayo−Illinois Alliance for Technology Based Health Care (http://mayoillinois.org/). Finally, the authors also thank Drs. A. Bird for the MBD1x expression vector, previously referred to as 1xMBD,[44] and Prof. P. Soloway at Cornell University for technical advice on purification of the MBD1x protein providing the coding sequence for MBD1x.

Supporting Information Available: Figures corresponding to experiments and complementary results. This material is available free of charge *via* the Internet at http://pubs.acs.org.

REFERENCES AND NOTES

1. Fearon, E. R.; Vogelstein, B. A Genetic Model for Colorectal Tumorigenesis. *Cell* **1990**, *61*, 759–767.
2. Baylin, S. B.; Herman, J. G.; Graff, J. R.; Vertino, P. M.; Issa, J. P. Alterations in DNA Methylation: A Fundamental Aspect of Neoplasia. *Adv. Cancer Res.* **1998**, *72*, 141–196.
3. Li, E.; Bestor, T. H.; Jaenisch, R. Targeted Mutation of the DNA Methyltransferase Gene Results in Embryonic Lethality. *Cell* **1992**, *69*, 915–926.
4. Laird, P. W. The Power and the Promise of DNA Methylation Markers. *Nat. Rev. Cancer* **2003**, *3*, 253–266.
5. Laird, P. W.; Jaenisch, R. The Role of DNA Methylation in Cancer Genetics and Epigenetics. *Annu. Rev. Genet.* **1996**, *30*, 441–464.
6. Esteller, M.; Corn, P. G.; Baylin, S. B.; Herman, J. G. A Gene Hypermethylation Profile of Human Cancer. *Cancer Res.* **2001**, *61*, 3225–3229.
7. Das, P. M.; Singal, R. DNA Methylation and Cancer. *J. Clin. Oncol.* **2004**, *22*, 4632–4642.
8. Iqbal, S. M.; Akin, D.; Bashir, R. Solid-State Nanopore Channels with DNA Selectivity. *Nat. Nanotechnol.* **2007**, *2*, 243–248.
9. Strathdee, G.; Brown, R. Aberrant DNA Methylation in Cancer: Potential Clinical Interventions. *Expert Rev. Mol. Med.* **2002**, *4*, 1–17.
10. Vanaja, D. K.; Ehrich, M.; Van den Boom, D.; Cheville, J. C.; Karnes, R. J.; Tindall, D. J.; Cantor, C. R.; Young, C. Y. Hypermethylation of Genes for Diagnosis and Risk Stratification of Prostate Cancer. *Cancer Invest.* **2009**, *27*, 549–560.
11. Adorjan, P.; Distler, J.; Lipscher, E.; Model, F.; Muller, J.; Pelet, C.; Braun, A.; Florl, A. R.; Gutig, D.; Grabs, G.; et al. Tumour Class Prediction and Discovery by Microarray-Based DNA Methylation Analysis. *Nucleic Acids Res.* **2002**, *30*, e21.
12. Iacobuzio-Donahue, C. A.; Maitra, A.; Olsen, M.; Lowe, A. W.; Van Heek, N. T.; Rosty, C.; Walter, K.; Sato, N.; Parker, A.; Ashfaq, R.; et al. Exploration of Global Gene Expression Patterns in Pancreatic Adenocarcinoma Using cDNA Microarrays. *Am. J. Pathol.* **2003**, *162*, 1151–1162.
13. Goelz, S. E.; Vogelstein, B.; Hamilton, S. R.; Feinberg, A. P. Hypomethylation of DNA from Benign and Malignant Human-Colon Neoplasms. *Science* **1985**, *228*, 187–190.
14. Feinberg, A. P.; Gehrke, C. W.; Kuo, K. C.; Ehrlich, M. Reduced Genomic 5-Methylcytosine Content in Human Colonic Neoplasia. *Cancer Res.* **1988**, *48*, 1159–1161.
15. Oshimo, Y.; Nakayama, H.; Ito, R.; Kitadai, Y.; Yoshida, K.; Chayama, K.; Yasui, W. Promoter Methylation of Cyclin D2 Gene in Gastric Carcinoma. *Int. J. Oncol.* **2003**, *23*, 1663–1670.
16. Akiyama, Y.; Maesawa, C.; Ogasawara, S.; Terashima, M.; Masuda, T. Cell-Type-Specific Repression of the Maspin Gene Is Disrupted Frequently by Demethylation at the Promoter Region in Gastric Intestinal Metaplasia and Cancer Cells. *Am. J. Pathol.* **2003**, *163*, 1911–1919.
17. Cho, M.; Uemura, H.; Kim, S. C.; Kawada, Y.; Yoshida, K.; Hirao, Y.; Konishi, N.; Saga, S.; Yoshikawa, K. Hypomethylation of the Mn/Ca9 Promoter and Upregulated Mn/Ca9 Expression in Human Renal Cell Carcinoma. *Br. J. Cancer* **2001**, *85*, 563–567.
18. Nakamura, N.; Takenaga, K. Hypomethylation of the Metastasis-Associated S100a4 Gene Correlates with Gene Activation in Human Colon Adenocarcinoma Cell Lines. *Clin. Exp. Metastasis* **1998**, *16*, 471–479.
19. Badal, V.; Chuang, L. S. H.; Tan, E. H. H.; Badal, S.; Villa, L. L.; Wheeler, C. A.; Li, B. F. L.; Bernard, H. U. Cpg Methylation of Human Papillomavirus Type 16 DNA in Cervical Cancer Cell Lines and in Clinical Specimens: Genomic Hypomethylation Correlates with Carcinogenic Progression. *J. Virol.* **2003**, *77*, 6227–6234.

20. De Capoa, A.; Musolino, A.; Della Rosa, S.; Caiafa, P.; Mariani, L.; Del Nonno, F.; Vocaturo, A.; Donnorso, R. P.; Niveleau, A.; Grappelli, C. DNA Demethylation Is Directly Related to Tumour Progression: Evidence in Normal, Pre-malignant and Malignant Cells from Uterine Cervix Samples. *Oncol. Rep.* **2003**, *10*, 545–549.
21. Sato, N.; Maitra, A.; Fukushima, N.; van Heek, N. T.; Matsubayashi, H.; Iacobuzio-Donahue, C. A.; Rosty, C.; Goggins, M. Frequent Hypomethylation of Multiple Genes Overexpressed in Pancreatic Ductal Adenocarcinoma. *Cancer Res.* **2003**, *63*, 4158–4166.
22. Piyathilake, C. J.; Henao, O.; Frost, A. R.; Macaluso, M.; Bell, W. C.; Johanning, G. L.; Heimburger, D. C.; Niveleau, A.; Grizzle, W. E. Race- and Age-Dependent Alterations in Global Methylation of DNA in Squamous Cell Carcinoma of the Lung (United States). *Cancer, Causes Control, Pap. Symp.* **2003**, *14*, 37–42.
23. Zou, H. Z.; Taylor, W. R.; Harrington, J. J.; Hussain, F. T. N.; Cao, X. M.; Loprinzi, C. L.; Levine, T. R.; Rex, D. K.; Ahnen, D.; Knigge, K. L.; et al. High Detection Rates of Colorectal Neoplasia by Stool DNA Testing with a Novel Digital Melt Curve Assay. *Gastroenterology* **2009**, *136*, 459–470.
24. Kisiel, J. B.; Yab, T. C.; Taylor, W. R.; Chari, S. T.; Petersen, G. M.; Mahoney, D. W.; Ahlquist, D. A. Stool DNA Testing for the Detection of Pancreatic Cancer Assessment of Methylation Marker Candidates. *Cancer* **2012**, *118*, 2623–2631.
25. Kandimalla, R.; van Tilborg, A. A.; Zwarthoff, E. C. DNA Methylation-Based Biomarkers in Bladder Cancer. *Nat. Rev. Urol.* **2013**, *10*, 327–335.
26. Jahr, S.; Hentze, H.; Englisch, S.; Hardt, D.; Fackelmayer, F. O.; Hesch, R. D.; Knippers, R. DNA Fragments in the Blood Plasma of Cancer Patients: Quantitations and Evidence for Their Origin from Apoptotic and Necrotic Cells. *Cancer Res.* **2001**, *61*, 1659–1665.
27. Mouliere, F.; Robert, B.; Peyrotte, E. A.; Del Rio, M.; Ychou, M.; Molina, F.; Gongora, C.; Thierry, A. R. High Fragmentation Characterizes Tumour-Derived Circulating DNA. *PLoS One* **2011**, *6*, e23418.
28. Murrell, A.; Rakyan, V. K.; Beck, S. From Genome to Epigenome. *Hum. Mol. Genet.* **2005**, *14*, R3–R10.
29. Grunau, C.; Renault, E.; Rosenthal, A.; Roizes, G. Methdb—A Public Database for DNA Methylation Data. *Nucleic Acids Res.* **2001**, *29*, 270–274.
30. Tian, K.; He, Z. J.; Wang, Y.; Chen, S. J.; Gu, L. Q. Designing a Polycationic Probe for Simultaneous Enrichment and Detection of Micrornas in a Nanopore. *ACS Nano* **2013**, *7*, 3962–3969.
31. Kang, I.; Wang, Y.; Reagan, C.; Fu, Y. M.; Wang, M. X.; Gu, L. Q. Designing DNA Interstrand Lock for Locus-Specific Methylation Detection in a Nanopore. *Sci. Rep.* **2013**, *3*, 2381.
32. Wang, Y.; Zheng, D. L.; Tan, Q. L.; Wang, M. X.; Gu, L. Q. Nanopore-Based Detection of Circulating Micrornas in Lung Cancer Patients. *Nat. Nanotechnol.* **2011**, *6*, 668–674.
33. Shim, J.; Humphreys, G. I.; Venkatesan, B. M.; Munz, J. M.; Zou, X. Q.; Sathe, C.; Schulten, K.; Kosari, F.; Nardulli, A. M.; Vasmatzis, G.; et al. Detection and Quantification of Methylation in DNA Using Solid-State Nanopores. *Sci. Rep.* **2013**, *3*, 1389.
34. Shim, J.; Gu, L. Q. Single-Molecule Investigation of G-Quadruplex Using a Nanopore Sensor. *Methods* **2012**, *57*, 40–46.
35. Gu, L. Q.; Shim, J. W. Single Molecule Sensing by Nanopores and Nanopore Devices. *Analyst* **2010**, *135*, 441–451.
36. Shasha, C.; Henley, R. Y.; Stoloff, D. H.; Rynearson, K. D.; Hermann, T.; Wanunu, M. Nanopore-Based Conformational Analysis of a Viral RNA Drug Target. *ACS Nano* **2014**, *8*, 6425–6430.
37. Kurz, V.; Nelson, E. M.; Shim, J.; Timp, G. Direct Visualization of Single-Molecule Translocations through Synthetic Nanopores Comparable in Size to a Molecule. *ACS Nano* **2013**, *7*, 4057–4069.
38. Carlsen, A. T.; Zahid, O. K.; Ruzicka, J. A.; Taylor, E. W.; Hall, A. R. Selective Detection and Quantification of Modified DNA with Solid-State Nanopores. *Nano Lett.* **2014**, *14*, 5488–5492.
39. Branton, D.; Deamer, D. W.; Marziali, A.; Bayley, H.; Benner, S. A.; Butler, T.; Di Ventra, M.; Garaj, S.; Hibbs, A.; Huang, X. H.; et al. The Potential and Challenges of Nanopore Sequencing. *Nat. Biotechnol.* **2008**, *26*, 1146–1153.
40. Venkatesan, B. M.; Bashir, R. Nanopore Sensors for Nucleic Acid Analysis. *Nat. Nanotechnol.* **2011**, *6*, 615–624.
41. Wanunu, M.; Cohen-Karni, D.; Johnson, R. R.; Fields, L.; Benner, J.; Peterman, N.; Zheng, Y.; Klein, M. L.; Drndic, M. Discrimination of Methylcytosine from Hydroxymethylcytosine in DNA Molecules. *J. Am. Chem. Soc.* **2011**, *133*, 486–492.
42. Shim, J.; Rivera, J.; Bashir, R. Electron Beam Induced Local Crystallization of HfO_2 Nanopores for Biosensing Applications. *Nanoscale* **2013**, *5*, 10887–10893.
43. Venkatesan, B. M.; Dorvel, B.; Yemenicioglu, S.; Watkins, N.; Petrov, I.; Bashir, R. Highly Sensitive, Mechanically Stable Nanopore Sensors for DNA Analysis. *Adv. Mater.* **2009**, *21*, 2771–2776.
44. Jorgensen, H. F.; Adie, K.; Chaubert, P.; Bird, A. P. Engineering a High-Affinity Methyl-Cpg-Binding Protein. *Nucleic Acids Res.* **2006**, *34*, e96.
45. Buck-Koehntop, B. A.; Martinez-Yamout, M. A.; Dyson, H. J.; Wright, P. E. Kaiso Uses All Three Zinc Fingers and Adjacent Sequence Motifs for High Affinity Binding to Sequence-Specific and Methyl-Cpg DNA Targets. *FEBS Lett.* **2012**, *586*, 734–739.
46. Bowers, P. M.; Schaufler, L. E.; Klevit, R. E. A Folding Transition and Novel Zinc Finger Accessory Domain in the Transcription Factor Adr1. *Nat. Struct. Biol.* **1999**, *6*, 478–485.
47. Drew, H. R.; Wing, R. M.; Takano, T.; Broka, C.; Tanaka, S.; Itakura, K.; Dickerson, R. E. Structure of a B-DNA Dodecamer: Conformation and Dynamics. *Proc. Natl. Acad. Sci. U.S.A.* **1981**, *78*, 2179–2183.
48. Ohki, I.; Shimotake, N.; Fujita, N.; Jee, J.; Ikegami, T.; Nakao, M.; Shirakawa, M. Solution Structure of the Methyl-Cpg Binding Domain of Human Mbd1 in Complex with Methylated DNA. *Cell* **2001**, *105*, 487–497.
49. Cerf, A.; Cipriany, B. R.; Benitez, J. J.; Craighead, H. G. Single DNA Molecule Patterning for High-Throughput Epigenetic Mapping. *Anal. Chem.* **2011**, *83*, 8073–8077.
50. Smeets, R. M. M.; Kowalczyk, S. W.; Hall, A. R.; Dekker, N. H.; Dekker, C. Translocation of Reca-Coated Double-Stranded DNA through Solid-State Nanopores. *Nano Lett.* **2009**, *9*, 3089–3095.
51. Wanunu, M.; Sutin, J.; McNally, B.; Chow, A.; Meller, A. DNA Translocation Governed by Interactions with Solid-State Nanopores. *Biophys. J.* **2008**, *95*, 4716–4725.
52. Zou, H. Z.; Harrington, J.; Rego, R. L.; Ahlquist, D. A. A Novel Method To Capture Methylated Human DNA from Stool: Implications for Colorectal Cancer Screening. *Clin. Chem.* **2007**, *53*, 1646–1651.
53. Carlsen, A. T.; Zahid, O. K.; Ruzicka, J.; Taylor, E. W.; Hall, A. R. Interpreting the Conductance Blockades of DNA Translocations through Solid-State Nanopores. *ACS Nano* **2014**, *8*, 4754–4760.
54. Ehrlich, M. DNA Hypomethylation in Cancer Cells. *Epigenomics* **2009**, *1*, 239–259.
55. Krausz, C.; Sandoval, J.; Sayols, S.; Chianese, C.; Giachini, C.; Heyn, H.; Esteller, M. Novel Insights into DNA Methylation Features in Spermatozoa: Stability and Peculiarities. *PLoS One* **2012**, *7*, e44479.
56. Lopes, E. C.; Valls, E.; Figueroa, M. E.; Mazur, A.; Meng, F. G.; Chiosis, G.; Laird, P. W.; Schreiber-Agus, N.; Greally, J. M.; Prokhortchouk, E.; et al. Kaiso Contributes to DNA Methylation-Dependent Silencing of Tumor Suppressor Genes in Colon Cancer Cell Lines. *Cancer Res.* **2008**, *68*, 7258–7263.
57. Strichman-Almashanu, L. Z.; Lee, R. S.; Onyango, P. O.; Perlman, E.; Flam, F.; Frieman, M. B.; Feinberg, A. P. A Genome-Wide Screen for Normally Methylated Human Cpg Islands That Can Identify Novel Imprinted Genes. *Genome Res.* **2002**, *12*, 543–554.
58. Wanunu, M.; Morrison, W.; Rabin, Y.; Grosberg, A. Y.; Meller, A. Electrostatic Focusing of Unlabelled DNA into

Nanoscale Pores Using a Salt Gradient. *Nat. Nanotechnol.* **2010**, *5*, 160–165.
59. Ahlquist, D. A.; Zou, H.; Domanico, M.; Mahoney, D. W.; Yab, T. C.; Taylor, W. R.; Butz, M. L.; Thibodeau, S. N.; Rabeneck, L.; Paszat, L. F.; et al. Next-Generation Stool DNA Test Accurately Detects Colorectal Cancer and Large Adenomas. *Gastroenterology* **2012**, *142*, 248–256.
60. Kim, Y.; Kim, S. H.; Ferracane, D.; Katzenellenbogen, J. A.; Schroeder, C. M. Specific Labeling of Zinc Finger Proteins Using Noncanonical Amino Acids and Copper-Free Click Chemistry. *Bioconjugate Chem.* **2012**, *23*, 1891–1901.